Quantum Acoustomechanics with a Micromagnet

Carlos Gonzalez-Ballestero,[1,2,*] Jan Gieseler,[3,4] and Oriol Romero-Isart[1,2]
[1]Institute for Quantum Optics and Quantum Information of the Austrian Academy of Sciences, A-6020 Innsbruck, Austria
[2]Institute for Theoretical Physics, University of Innsbruck, A-6020 Innsbruck, Austria
[3]Department of Physics, Harvard University, 17 Oxford Street, Cambridge, Massachusetts 02138, USA
[4]ICFO-Institut de Ciencies Fotoniques, Mediterranean Technology Park, 08860 Castelldefels (Barcelona), Spain

(Received 8 August 2019; accepted 6 February 2020; published 3 March 2020)

We show theoretically how to strongly couple the center-of-mass motion of a micromagnet in a harmonic potential to one of its acoustic phononic modes. The coupling is induced by a combination of an oscillating magnetic field gradient and a static homogeneous magnetic field. The former parametrically couples the center-of-mass motion to a magnonic mode while the latter tunes the magnonic mode in resonance with a given acoustic phononic mode. The magnetic fields can be adjusted to either cool the center-of-mass motion to the ground state or to enter into the strong quantum coupling regime. The center of mass can thus be used to probe and manipulate an acoustic mode, thereby opening new possibilities for out-of-equilibrium quantum mesoscopic physics. Our results hold for experimentally feasible parameters and apply to levitated micromagnets as well as micromagnets deposited on a clamped nanomechanical oscillator.

DOI: 10.1103/PhysRevLett.124.093602

In quantum optomechanics, coupling the mechanical mode of a macroscopic object to a low entropy and narrow mode of the electromagnetic field has enabled ground-state cooling of micromechanical oscillators both in the optical and in the microwave regime [1,2]. In addition, strong optomechanical coupling has allowed us to generate entanglement between micromechanical and electromagnetic modes [3,4], as well as entanglement between remote micromechanical oscillators [5]. In this Letter, we propose a novel analog to linearized quantum optomechanics [6] that does not require us to couple the mechanical oscillator to an electromagnetic field mode. Instead, we propose to couple the micromechanical oscillator to its internal quantum degrees of freedom.

Our proposal considers the center-of-mass motion of a micromagnet, which is either levitated [7–11] or attached to a high-Q micromechanical oscillator [12–16]; see Fig. 1(a). In the presence of properly tuned magnetic fields, we show how the inherent strong magnetoelastic coupling in the micromagnet can be utilized to achieve an *acoustomechanical* coupling between the center-of-mass motion of the micromagnet and one of its internal acoustic phononic modes. We show how both ground-state cooling and strong quantum acoustomechanical coupling can be achieved with experimentally feasible parameters. Our proposal thus establishes a method to probe and control collective quantum excitations of a levitated nanoparticle, thereby opening new possibilities for studying out-of-equilibrium quantum mesoscopic physics, such as, e.g., internal equilibration and radiative cooling with a levitated nanoparticle [17].

We consider a spherical micromagnet of radius R trapped in a harmonic potential, assumed nonmagnetic for simplicity. The micromagnet interacts with an external magnetic field, which has a homogeneous component $\mathbf{B}_0 = B_0\mathbf{e}_z$, and an oscillating gradient

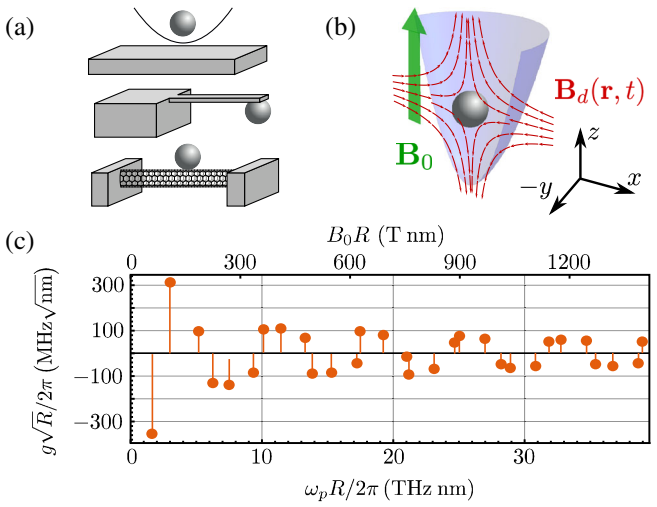

FIG. 1. (a),(b) Schematic illustration of our proposal. (c) Magnetoelastic coupling strength between the Kittel magnon and the first 30 acoustic spheroidal modes with angular (azimuthal) mode number 2 (1) versus acoustic mode frequency. The upper scale indicates the B_0 needed to tune magnon and phonon in resonance. All axes are normalized to be independent on the micromagnet radius R. Parameters correspond to yttrium iron garnet (YIG): $\rho_m = 5170\ \text{kg/m}^3$, $M_S = 5.87 \times 10^5\ \text{A/m}$, $|\gamma| = 1.76 \times 10^{11}\ \text{T}^{-1}\ \text{s}^{-1}$ [18,19].

$\mathbf{B}_d(\mathbf{r},t) = b_g(-x\mathbf{e}_x + z\mathbf{e}_z)\cos(\omega_d t)$, with $b_g R \ll B_0$ [Fig. 1(b)]. The Hamiltonian describing the dynamics of the relevant coupled degrees of freedom of the micromagnet is given by

$$\frac{\hat{H}(t)}{\hbar} = \omega_x \hat{b}^\dagger \hat{b} + \omega_m \hat{s}^\dagger \hat{s} + \omega_p \hat{a}^\dagger \hat{a} + g(\hat{s}^\dagger \hat{a} + \hat{s}\hat{a}^\dagger) + G_x \cos(\omega_d t)(\hat{s}^\dagger + \hat{s})(\hat{b}^\dagger + \hat{b}). \quad (1)$$

The first three terms describe, using bosonic operators, the free dynamics of the center-of-mass motion along the x axis ($\hat{b}$), the magnonic mode ($\hat{s}$), and an acoustic mode ($\hat{a}$) whose frequency is close to the magnonic mode frequency. The fourth term corresponds to the magnetoelastic coupling between the magnon and the acoustic phonon, whereas the last term describes the time-dependent coupling between the magnon and the center-of-mass motion due to the inhomogeneous drive $\mathbf{B}_d(\mathbf{r},t)$. Similar field inhomogeneities have been exploited to couple internal and external degrees of freedom in levitated nanodiamonds [20–23].

The Hamiltonian Eq. (1) is obtained as follows; see Ref. [24] for further details. First, one quantizes spin waves in a spherical micromagnet around the equilibrium point induced by $\mathbf{B}_0$, employing the dipolar, isotropic, and magnetostatic approximations [19,25–27], which are valid for micromagnet sizes 10 nm $\lesssim R \lesssim$ 1 cm. We focus on the Kittel magnonic mode, which corresponds to a homogeneous magnetization precessing around the z axis with frequency $\omega_m = |\gamma| B_0$, where γ is the gyromagnetic ratio. Second, one quantizes linear elastic waves in a sphere [28,29], obtaining analytical expressions for the acoustic modes with frequencies proportional to R^{-1}. Within this linear theory, elastic waves and center-of-mass motion are uncoupled. Third, the magnetoelastic interaction is calculated [18,30], and, for nanometer- and micrometer-sized magnets, the leading contribution is of quadratic form. In addition, one obtains selection rules showing that the Kittel mode only couples to acoustic phononic modes of the family S_{n21}, that is, spheroidal modes with fixed angular (azimuthal) mode index 2 (1) and arbitrary radial positive integer index n. By tuning B_0 such that the Kittel magnon frequency ω_m is close to the resonance frequency of an acoustic mode S_{n21}, and using the rotating wave approximation, valid for sufficiently small coupling rate and magnon-phonon detuning, the magnetoelastic interaction is described by the beam-splitter form given in Eq. (1). The scaled coupling rate ($g \propto R^{-1/2}$) is shown in Fig. 1(c) for $n = 1, \ldots, 30$, which also evidences the well-discretized spectrum of the acoustic phonons. Finally, the interaction between the center-of-mass motion and the Kittel magnon, namely the last term in Eq. (1), is obtained from the micromagnetic energy density term accounting for the magnetic dipolar coupling with $\mathbf{B}_d(\mathbf{r},t)$. Assuming the motional amplitude of the center of mass to be much smaller than B_0/b_g, the R-independent coupling rate is given by $G_x = b_g V \mathcal{M}_K x_0/(2\hbar)$, where V is the volume of the micromagnet, $\mathcal{M}_K = \sqrt{\hbar|\gamma|M_S/2V}$ the zero-point magnetization of the Kittel magnon, M_S the saturation magnetization [19,27], and $x_0 = [2\rho_m V \omega_x/\hbar]^{-1/2}$ the zero-point motion of the center-of-mass oscillation along the x axis, where ρ_m is the mass density of the micromagnet [31].

The system dynamics is described by the master equation $\dot{\hat{\rho}} = (i\hbar)^{-1}[\hat{H},\hat{\rho}] + \mathcal{L}[\hat{\rho}]$, where $\hat{\rho}$ is the density operator and $\mathcal{L}[\hat{\rho}] = \mathcal{L}_m[\hat{\rho}] + \mathcal{L}_p[\hat{\rho}] + \mathcal{L}_x[\hat{\rho}]$ accounts for the unavoidable dissipation. Such dissipators, for $j = m, p, x$, are given by $\mathcal{L}_j[\hat{\rho}] = \gamma_j[(\bar{n}_j + 1)L_{\hat{o}_j} + \bar{n}_j L_{\hat{o}_j^\dagger}]$, where for compactness we define $\{\hat{o}_m, \hat{o}_p, \hat{o}_x\} \equiv \{\hat{s}, \hat{a}, \hat{b}\}$ and $L_{\hat{o}}[\hat{\rho}] \equiv \hat{o}\,\hat{\rho}\,\hat{o}^\dagger - \{\hat{o}^\dagger\hat{o}, \hat{\rho}\}/2$. We have introduced the decay rate γ_j and thermal occupation number $\bar{n}_j = (\exp[\hbar\omega_j/k_B T_{e,j}] - 1)^{-1}$, where k_B is the Boltzmann constant and $T_{e,j}$ is the temperature of the thermal environment of each degree of freedom. The above master equation is quadratic and can thus be solved exactly. It is convenient to define mechanical and acoustic quality factors as $Q_x \equiv \omega_x/\gamma_x$ and $Q_p \equiv \omega_p/\gamma_p$, respectively. Experimental values for Q_x exceed $Q_x \gtrsim 10^8$ both in nanofabricated resonators [32–35] and in levitated systems [36,37]. Regarding Q_p, unusually high values ($Q_p \approx 10^5$–10^7) have been reported in millimeter-sized yttrium iron garnet (YIG) spheres [18,38], but no measurements have been performed for isolated micromagnets of the sizes considered in this Letter. However, for sufficiently isolated mechanical microresonators, Q_p is known to be limited by indirect interactions with other acoustic modes, and reaches values up to $Q_p \gtrsim 5 \times 10^{10}$ [18,39] when consecutive acoustic modes are far detuned ($\gtrsim$GHz). Therefore, one might expect values of Q_p as high as $\sim 10^{10}$ in our system.

To discuss the center-of-mass dynamics, it is convenient to diagonalize the magnon-phonon Hamiltonian through a Bogoliubov transformation, $\omega_m \hat{s}^\dagger \hat{s} + \omega_p \hat{a}^\dagger \hat{a} + g(\hat{s}^\dagger \hat{a} + \text{H.c.}) = \sum_{\alpha=1,2} \omega_\alpha \hat{c}_\alpha^\dagger \hat{c}_\alpha$. The new normal modes are hybrid magnon-phonon excitations given by $\hat{c}_1 = (\hat{s} - \chi\hat{a})/\mathcal{N}$ and $\hat{c}_2 = -(\chi\hat{s} + \hat{a})/\mathcal{N}$, where $\mathcal{N} \equiv \sqrt{1+\chi^2}$, $\chi \equiv -2g/[\Delta - (\Delta^2 + 4g^2)^{1/2}]$, and $\Delta \equiv \omega_m - \omega_p$. The phonon (magnon) fraction in mode $\hat{c}_1$ ($\hat{c}_2$) is given by $(\chi/\mathcal{N})^2$. Both the factor $\chi \in [0, \infty)$ and the eigenfrequencies $2\omega_\alpha = \omega_m + \omega_p + (-1)^\alpha(\Delta^2 + 4g^2)^{1/2}$ are fully tunable through the external field B_0. In terms of the normal modes and in the rotating frame, $\hat{U}(t) = \exp(i\omega_d t \sum_\alpha \hat{c}_\alpha^\dagger \hat{c}_\alpha)$, the Hamiltonian Eq. (1) reads

$$\frac{\hat{H}}{\hbar} = \omega_x \hat{b}^\dagger \hat{b} + \sum_{\alpha=1,2} \Delta_\alpha \hat{c}_\alpha^\dagger \hat{c}_\alpha + (\hat{b}^\dagger + \hat{b}) \sum_{\alpha=1,2} (G_{x\alpha} \hat{c}_\alpha^\dagger + \text{H.c.}), \quad (2)$$

after a rotating wave approximation, valid for $\omega_d \gg |G_x|/4, \omega_x$. Here $\Delta_\alpha \equiv \omega_\alpha - \omega_d$, and the couplings are renormalized to $G_{x1} = G_x/(2\mathcal{N})$ and $G_{x2} = -\chi G_{x1}$. In terms of the normal modes, the dissipators take the form $\mathcal{L}_p[\hat{\rho}] + \mathcal{L}_m[\hat{\rho}] = \mathcal{L}_{12}[\hat{\rho}] + \sum_{\alpha=1,2}(\gamma_{\alpha+}L_{\hat{c}_\alpha^\dagger}[\hat{\rho}] + \gamma_{\alpha-}L_{\hat{c}_\alpha}[\hat{\rho}])$. The $\mathcal{L}_{12}$ term describes an incoherent interaction which can be neglected, under a rotating wave approximation, for micromagnet radii $R \lesssim 10$ μm [24]. The corresponding rates in the remaining terms are given by $\gamma_{1\xi} = \Gamma_{m\xi} + \chi^2\Gamma_{p\xi}$ and $\gamma_{2\xi} = \chi^2\Gamma_{m\xi} + \Gamma_{p\xi}$, with $\Gamma_{m\xi} \equiv \gamma_m(\bar{n}_m + \delta_{\xi-})/\mathcal{N}^2$ and $\Gamma_{p\xi} \equiv \gamma_p(\bar{n}_p + \delta_{\xi-})/\mathcal{N}^2$. Here $\xi = +, -$ and $\delta_{\xi\xi'}$ is a Kronecker delta. We define the linewidth of the mode $\hat{c}_1$ [$\hat{c}_2$] as $\gamma_1 \equiv (\gamma_m + \gamma_p\chi^2)/\mathcal{N}^2$ [$\gamma_2 \equiv (\gamma_m\chi^2 + \gamma_p)/\mathcal{N}^2$]. Note that in terms of the normal modes, the center of mass is coupled to two independent, largely detuned modes, as $\Delta_1 - \Delta_2 = 2(\Delta^2 + 4g^2)^{1/2} \gg \omega_x$ for typical mechanical frequencies. To maximize the acoustomechanical interaction, the magnetic field parameters B_0 and ω_d are adjusted such that mode $\hat{c}_2$ is in resonance with the center-of-mass motion ($\Delta_2 = \omega_x$) and $\chi = 10^{-2}$, so that $\hat{c}_2$ is mainly ($\approx$99.99%) acoustic [40]. The associated decrease in the coupling between $\hat{c}_2$ and the center of mass, $G_{x2} \propto \chi$, can be independently compensated by increasing the field gradient b_g. In this way, we form a quasi-two-mode acoustomechanical system where the mechanical motion of the micromagnet is coupled to the mainly (99.99%) acoustic $\hat{c}_2$ mode, which plays the role of the electromagnetic mode in optomechanics [6].

In order to explore the physical regimes that our proposed acoustomechanical system can achieve, we plot the ratio $|G_{x2}|/\gamma_2 \propto b_g$ in Fig. 2(a) (left axis), the ratio ω_x/γ_2 in Fig. 2(a) (right axis), and the cooperativity $C \equiv 4G_{x2}^2/(\gamma_2\gamma_x) \propto b_g^2$ in Fig. 2(b), as a function of the acoustic quality factor Q_p and for three values of the micromagnet radius R. Hereafter, we consider the lowest-order (S_{121}) phonon, material parameters for YIG, and fix $\omega_x = 2\pi \times$ 200 kHz and $\gamma_m = 2\pi \times 1$ MHz [41]. All the quantities in Fig. 2 increase initially as a function of Q_p, as the linewidth $\gamma_2 \approx \gamma_m\chi^2 + \omega_p/Q_p$ is reduced, and saturate for large Q_p where $\gamma_2 \to \chi^2\gamma_m$ becomes magnon-limited. The system resides both in the resolved-sideband regime ($\omega_x > \gamma_2$) and the high-cooperativity ($C > 1$) regime even at moderate $Q_p \sim 10^6$ and magnetic field gradients $b_g \sim 5$ T/m. The strong-coupling regime ($|G_{x2}| > \gamma_2$) can also be attained for a wide range of Q_p and feasible gradients $b_g \sim 10^3$–10^4 T/m. Moreover, the system can reach the strong quantum cooperativity regime $C/(\bar{n}_x\bar{n}_p) > 1$ allowing for coherent quantum state transfer between mechanical motion and acoustic phonons [6]. Indeed, at cryogenic temperatures ($T_{e,j} = 100$ mK), the product $\bar{n}_x\bar{n}_p < 10^4$ and $C/(\bar{n}_x\bar{n}_p) > 1$ can be achieved for $b_g \gtrsim 10^3$ T/m and $Q_p \gtrsim 10^6$ for all radii in Fig. 2. At room temperature, attaining such a regime is more challenging

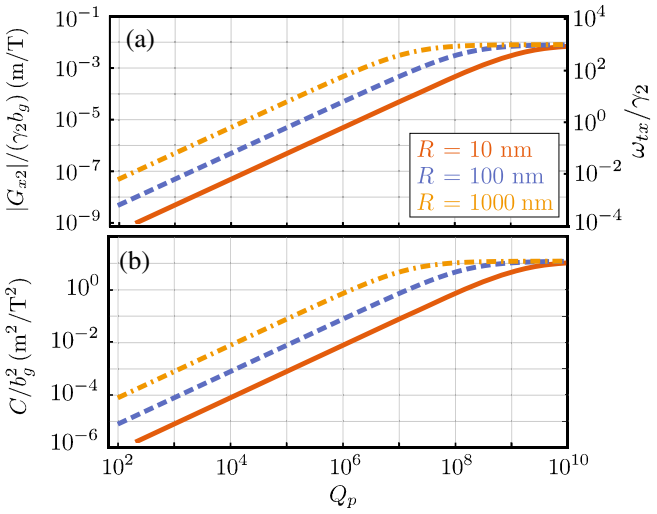

FIG. 2. Relevant acoustomechanical parameters for $Q_x = 10^8$ versus acoustic quality factor Q_p. The dependence with the field gradient b_g has been factored out explicitly, so the figures are b_g independent. (a) Coupling (left) and mechanical frequency (right) normalized to linewidth of mode $\hat{c}_2$. (b) Single-phonon cooperativity $C \equiv 4G_{x2}^2/\gamma_2\gamma_x$. In both panels we fix $\chi = 10^{-2}$ by applying an external static field $B_0 \approx \{5.4, 0.45, 0.018\}$ T for $R = \{10, 10^2, 10^3\}$ nm, respectively.

and only feasible for small R at gradients $\gtrsim 10^4$ T/m. Figure 2 highlights that our acoustomechanical system can be tuned into the resolved-sideband, the high-cooperativity, and either the weak- or the strong-coupling regime with experimentally accessible parameters. This versatility enables a range of applications, which we will discuss in the following.

Efficient center-of-mass cooling can be achieved in the resolved-sideband, high-cooperativity, and weak-coupling regime [42–44]. By solving the quadratic master equation exactly, the steady-state occupation of the center of mass $\langle\hat{b}^\dagger\hat{b}\rangle_{\rm ss}$ can be evaluated. Figure 3(a) [Fig. 3(b)] shows $\langle\hat{b}^\dagger\hat{b}\rangle_{\rm ss}$ for $R = 100$ nm [$R = 1$ μm] at $Q_x = 10^8$ and different field gradients b_g, for both a room temperature environment ($T_{e,j} = 300$ K, solid lines) and cryogenic conditions ($T_{e,j} = 100$ mK, dashed lines). For small acoustic quality factors, the cooling is inefficient as $C < 1$ (see Fig. 2). When Q_p increases above a certain value (which depends on R and b_g, see Fig. 2), the $C > 1$ regime is reached and center-of-mass cooling is observed. Notice that ground-state cooling, $\langle\hat{b}^\dagger\hat{b}\rangle_{\rm ss} < 1$, is achieved for both micromagnet sizes at $T_{e,j} = 100$ mK. For sufficiently high Q_p, however, the cooling becomes less efficient as the system enters the strong-coupling regime [42–44]. The lowest occupations in both panels of Fig. 3, i.e., the minima of the green dashed lines, correspond to parameters at which the mechanical sidebands are very well resolved ($\omega_x/\gamma_2 \sim 10^2$, see Fig. 2), and thus cooling is limited by

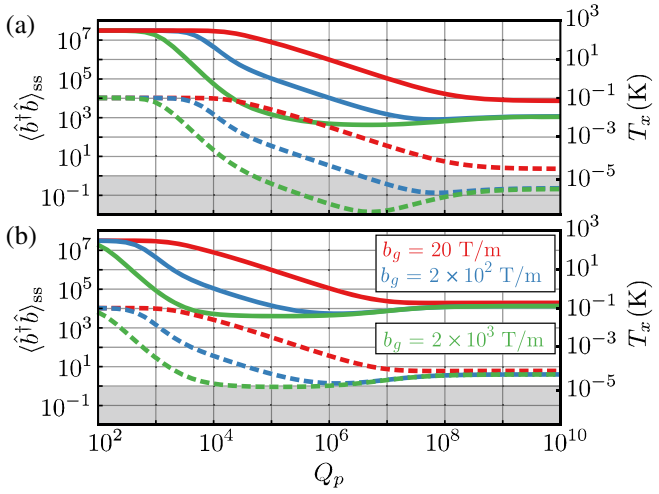

FIG. 3. Steady-state center-of-mass occupation ($Q_x = 10^8$) versus acoustic quality factor, for $R = 100$ nm (a) and $R = 1$ μm (b) and three values of the magnetic gradient b_g. Solid and dashed lines indicate results at room ($T_{e,j} = 300$ K) and cryogenic temperatures ($T_{e,j} = 100$ mK), respectively. The shaded area indicates the ground-state cooling region $\langle \hat{b}^\dagger \hat{b} \rangle_{ss} < 1$. The right-hand axes indicate the steady-state center-of-mass temperature $k_B T_x \approx \hbar \omega_x \langle \hat{b}^\dagger \hat{b} \rangle_{ss}$ ($\omega_x = 2\pi \times 200$ kHz).

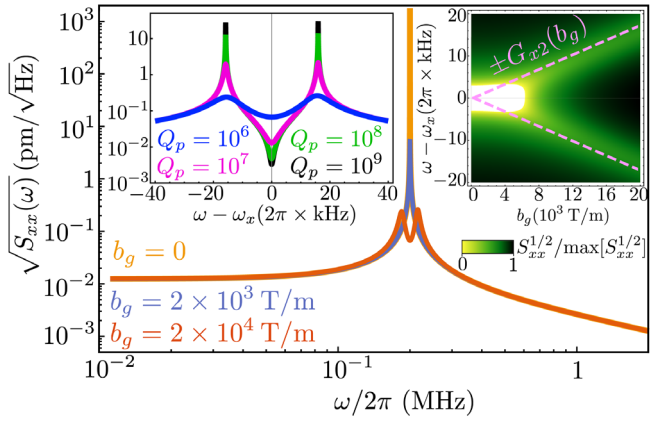

FIG. 4. Power spectral density $S_{xx}(\omega)$, for $Q_p = 10^6$, $Q_x = 10^5$, $R = 100$ nm, and $T_{e,j} = 300$ K, at three different values of the field gradient b_g. Left inset: Peak splitting at $b_g = 10^4$ T/m, for different acoustic quality factors Q_p. Right inset: Normalized power spectral density as a function of b_g and detuning $\omega - \omega_x$. The dashed lines indicate the function $\pm G_{x2}(b_g)$. Strong coupling is reached at $b_g \approx 10^4$ T/m.

other factors. For $R = 100$ nm, the lowest occupation $\langle \hat{b}^\dagger \hat{b} \rangle_{ss,min} \approx 0.014$ at $b_g = 2 \times 10^3$ T/m is cooperativity-limited. It can, thus, be reduced by increasing either b_g or Q_x. In contrast, for $R = 1$ μm, $\langle \hat{b}^\dagger \hat{b} \rangle_{ss,min} \approx 0.89$ at $b_g = 2 \times 10^3$ T/m is limited by the entropy of the acoustic phonon bath through the phonon occupation $\bar{n}_p$ [45], which increases with R due to the reduction of the acoustic frequency. Note that further cooling is still possible in this case by tuning the Kittel mode close to resonance with a higher order (lower entropy) acoustic phonon [24]; see Fig. 1(c). As evidenced by these results, coupling the micromagnet motion to its built-in internal resonators (i.e., phonons) allows for cavityless cooling of the motion, an especially promising prospect for levitated micromagnets for which neither optical cooling nor microwave optomechanical cooling are efficient, due to absorption and weak coupling rates, respectively.

The strong and tunable acoustomechanical interaction also allows us to probe the acoustic phonons by measuring the mechanical displacement of the center of mass. Figure 4 shows the power spectral density of the center-of-mass motion, $S_{xx}(\omega) \equiv (2\pi)^{-1} \int_{-\infty}^{\infty} d\tau \langle \hat{x}(0)\hat{x}(\tau) \rangle_{ss} e^{i\omega\tau}$, where $\hat{x} \equiv x_0(\hat{b}^\dagger + \hat{b})$, for $R = 100$ nm and moderate quality factors $Q_x = 10^5$ and $Q_p = 10^6$. For these parameters, $\omega_x/\gamma_2 \approx 10$ and $2|G_{x2}|/\gamma_2 \approx 10^{-4} b_g$ [see Fig. 2(a)]. We distinguish the three possible regimes in Fig. 4, namely, the zero-coupling regime ($b = 0$), where the single peak at $\omega = \omega_x$ and width $\gamma_x \approx 2\pi \times 2$ Hz indicates a freely evolving center-of-mass motion, the weak-coupling regime ($b_g = 2 \times 10^3$ T/m), characterized by a reduced peak, i.e., by cooling of the mechanical motion, and the strong-coupling regime ($b_g = 2 \times 10^4$ T/m), where the peak splits into two [46]. The latter splitting is induced exclusively by the mode $\hat{c}_2$, i.e., by acoustic phonons, as evidenced by the two insets of Fig. 4. In the left-hand inset we observe how the signal increases with the acoustic quality factor, up to the magnon-limited saturation point ($Q_p \sim 10^9$) (see also Fig. 2). The right-hand inset shows that the mode splitting is well approximated by the function $2|G_{x2}(b_g)|$. The strong-coupling crossover $2|G_{x2}(b_g)|/\gamma_2 = 1$ is at $b_g \approx 10^4$ T/m for the chosen parameters. Measuring the peak splitting due to the center of mass hybridizing with the acoustic mode requires to resolve the thermal motion of the center-of-mass mode. According to the results in Fig. 4, this lies well within the sensitivity range of most state-of-the-art ultrasensitive micromechanical sensors [36,47–51], which can even resolve motion on the quantum level [35,52,53]. Thus, the acoustic-induced mode splitting is experimentally measurable. Let us finally emphasize that, in all the above results, the internal temperature increase of the micromagnet remains low in spite of the magnetic driving, as such driving is largely detuned with respect to the magnon frequency [24].

In conclusion, we have shown that the center of mass of a micromagnet in a harmonic potential can be coupled, in a strong and tunable way, to one of its internal acoustic phononic modes. The coupling mechanism can be controlled by external magnetic fields and both ground-state cooling and the strong quantum coupling regime can be achieved. Such a quantum acoustomechanical system opens many possibilities for further research: (i) exploring the strong quantum cooperativity regime to use an internal

acoustic phonon as a quantum memory [39], (ii) preparing the micromagnet in a state where different acoustic modes have different temperatures and probe how they equilibrate [17], and (iii) exploring the regimes where the potentially strong nonlinear magnetoelastic interactions [24] might become relevant, to generate a nonlinear hybrid magnon-phonon mode. This mode can act as a qubit and can thus be used to prepare the center of mass in a non-Gaussian quantum state. Last but not least, in the context of levitated nanoparticles, our work highlights the important fact that nanoparticles are not point objects with only external degrees of freedom, but complex particles with internal degrees of freedom that can be harnessed in the quantum regime.

C. G.-B. and J. G. acknowledge support from the European Union (PWAQUTEC, H2020-MSCA-IF-2017, No. 796725 and SEQOO, H2020-MSCA-IF-2014, No. 655369, respectively).

*carlos.gonzalez-ballestero@uibk.ac.at

[1] J. D. Teufel, T. Donner, D. Li, J. W. Harlow, M. S. Allman, K. Cicak, A. J. Sirois, J. D. Whittaker, K. W. Lehnert, and R. W. Simmonds, Sideband cooling of micromechanical motion to the quantum ground state, Nature (London) **475**, 359 (2011).

[2] J. Chan, T. P. M. Alegre, A. H. Safavi-Naeini, J. T. Hill, A. Krause, S. Gröblacher, M. Aspelmeyer, and O. Painter, Laser cooling of a nanomechanical oscillator into its quantum ground state, Nature (London) **478**, 89 (2011).

[3] T. A. Palomaki, J. D. Teufel, R. W. Simmonds, and K. W. Lehnert, Entangling mechanical motion with microwave fields, Science **342**, 710 (2013).

[4] R. Riedinger, S. Hong, R. A. Norte, J. A. Slater, J. Shang, A. G. Krause, V. Anant, M. Aspelmeyer, and S. Gröblacher, Non-classical correlations between single photons and phonons from a mechanical oscillator, Nature (London) **530**, 313 (2016).

[5] R. Riedinger, A. Wallucks, I. Marinković, C. Löschnauer, M. Aspelmeyer, S. Hong, and S. Gröblacher, Remote quantum entanglement between two micromechanical oscillators, Nature (London) **556**, 473 (2018).

[6] M. Aspelmeyer, T. J. Kippenberg, and F. Marquardt, Cavity optomechanics, Rev. Mod. Phys. **86**, 1391 (2014).

[7] J. Prat-Camps, C. Teo, C. C. Rusconi, W. Wieczorek, and O. Romero-Isart, Ultrasensitive Inertial and Force Sensors with Diamagnetically Levitated Magnets, Phys. Rev. Applied **8**, 034002 (2017).

[8] C. C. Rusconi, V. Pöchhacker, K. Kustura, J. I. Cirac, and O. Romero-Isart, Quantum Spin Stabilized Magnetic Levitation, Phys. Rev. Lett. **119**, 167202 (2017).

[9] P. Huillery, T. Delord, L. Nicolas, M. Bossche, M. Perdriat, and G. Hétet, Spin-mechanics with levitating ferromagnetic particles, arXiv:1903.09699.

[10] H. Barowski, K. M. Sattler, and W. Schoepe, Static and dynamic forces on a permanent magnet levitating between superconducting surfaces, J. Low Temp. Phys. **93**, 85 (1993).

[11] J. Druge, C. Jean, O. Laurent, M.-A. Méasson, and I. Favero, Damping and non-linearity of a levitating magnet in rotation above a superconductor, New J. Phys. **16**, 075011 (2014).

[12] J. A. J. Burgess, A. E. Fraser, F. F. Sani, D. Vick, B. D. Hauer, J. P. Davis, and M. R. Freeman, Quantitative magneto-mechanical detection and control of the barkhausen effect, Science **339**, 1051 (2013).

[13] A. Vinante, G. Wijts, O. Usenko, L. Schinkelshoek, and T. H. Oosterkamp, Magnetic resonance force microscopy of paramagnetic electron spins at millikelvin temperatures, Nat. Commun. **2**, 572 (2011).

[14] N. Shamsudhin, Y. Tao, J. Sort, B. Jang, C. L. Degen, B. J. Nelson, and S. Pané, Magnetometry of individual polycrystalline ferromagnetic nanowires, Small **12**, 6363 (2016).

[15] R. Fischer, D. P. McNally, C. Reetz, G. G. T. Assumpção, T. Knief, Y. Lin, and C. A. Regal, Spin detection with a micromechanical trampoline: towards magnetic resonance microscopy harnessing cavity optomechanics, New J. Phys. **21**, 043049 (2019).

[16] S. Kolkowitz, A. C. Bleszynski Jayich, Q. P. Unterreithmeier, S. D. Bennett, P. Rabl, J. G. E. Harris, and M. D. Lukin, Coherent sensing of a mechanical resonator with a single-spin qubit, Science **335**, 1603 (2012).

[17] A. E. Rubio López, C. Gonzalez-Ballestero, and O. Romero-Isart, Internal quantum dynamics of a nanoparticle in a thermal electromagnetic field: A minimal model, Phys. Rev. B **98**, 155405 (2018).

[18] X. Zhang, C.-L. Zou, L. Jiang, and H. X. Tang, Cavity magnomechanics, Sci. Adv. **2**, e1501286 (2016).

[19] D. Stancil and A. Prabhakar, *Spin Waves: Theory and Applications* (Springer, New York, 2009).

[20] G. P. Conangla, A. W. Schell, R. A. Rica, and R. Quidant, Motion control and optical interrogation of a levitating single nitrogen vacancy in vacuum, Nano Lett. **18**, 3956 (2018).

[21] A. T. M. A. Rahman and P. F. Barker, Laser refrigeration, alignment and rotation of levitated Yb^{3+} : YLF nanocrystals, Nat. Photonics **11**, 634 (2017).

[22] T. Delord, P. Huillery, L. Schwab, L. Nicolas, L. Lecordier, and G. Hétet, Ramsey Interferences and Spin Echoes from Electron Spins Inside a Levitating Macroscopic Particle, Phys. Rev. Lett. **121**, 053602 (2018).

[23] T. M. Hoang, J. Ahn, J. Bang, and T. Li, Electron spin control of optically levitated nanodiamonds in vacuum, Nat. Commun. **7**, 12250 (2016).

[24] C. Gonzalez-Ballestero, D. Hümmer, J. Gieseler, and O. Romero-Isart, companion paper, Theory of quantum acoustomagnonics and acoustomechanics with a micromagnet, Phys. Rev. B **101**, 125404 (2020).

[25] L. R. Walker, Magnetostatic modes in ferromagnetic resonance, Phys. Rev. **105**, 390 (1957).

[26] P. C. Fletcher and R. O. Bell, Ferrimagnetic resonance modes in spheres, J. Appl. Phys. **30**, 687 (1959).

[27] D. Mills, Quantum theory of spin waves in finite samples, J. Magn. Magn. Mater. **306**, 16 (2006).

[28] A. Eringen and E. Suhubi, *Elastodynamics: Linear Theory* (Academic Press, New York, 1975), Vol. 2.

[29] H. Lamb, On the vibrations of an elastic sphere, Proc. London Math. Soc. **s1-13**, 189 (1881).

[30] L. Landau and E. Lifshitz, *Electrodynamics of Continuous Media*, 2nd. ed. (Pergamon, Amsterdam, 1984).
[31] Note that, in the case of a micromagnet deposited on a sufficiently massive micromechanical oscillator, the quantity $\rho_m V$ should be substituted by the effective mass of the oscillator.
[32] R. A. Norte, J. P. Moura, and S. Gröblacher, Mechanical Resonators for Quantum Optomechanics Experiments at Room Temperature, Phys. Rev. Lett. **116**, 147202 (2016).
[33] C. Reinhardt, T. Müller, A. Bourassa, and J. C. Sankey, Ultralow-Noise Sin Trampoline Resonators for Sensing and Optomechanics, Phys. Rev. X **6**, 021001 (2016).
[34] A. H. Ghadimi, S. A. Fedorov, N. J. Engelsen, M. J. Bereyhi, R. Schilling, D. J. Wilson, and T. J. Kippenberg, Elastic strain engineering for ultralow mechanical dissipation, Science **360**, 764 (2018).
[35] D. Mason, J. Chen, M. Rossi, Y. Tsaturyan, and A. Schliesser, Continuous force and displacement measurement below the standard quantum limit, Nat. Phys. **15**, 745 (2019).
[36] J. Gieseler, L. Novotny, and R. Quidant, Thermal nonlinearities in a nanomechanical oscillator, Nat. Phys. **9**, 806 (2013).
[37] J. Gieseler, B. Deutsch, R. Quidant, and L. Novotny, Subkelvin Parametric Feedback Cooling of a Laser-trapped Nanoparticle, Phys. Rev. Lett. **109**, 103603 (2012).
[38] R. C. LeCraw, E. G. Spencer, and E. I. Gordon, Extremely Low Loss Acoustic Resonance in Single-Crystal Garnet Spheres, Phys. Rev. Lett. **6**, 620 (1961).
[39] G. S. MacCabe, H. Ren, J. Luo, J. D. Cohen, H. Zhou, A. Sipahigil, M. Mirhosseini, and O. Painter, Phononic bandgap nano-acoustic cavity with ultralong phonon lifetime, arXiv:1901.04129.
[40] Note that although the roles of $\hat{c}_1$ and $\hat{c}_2$ could be exchanged by tuning the former in resonance to the center of mass and choosing a large χ, the present choice is preferred as it requires smaller fields B_0 [24].
[41] Y. Tabuchi, S. Ishino, T. Ishikawa, R. Yamazaki, K. Usami, and Y. Nakamura, Hybridizing Ferromagnetic Magnons and Microwave Photons in the Quantum Limit, Phys. Rev. Lett. **113**, 083603 (2014).
[42] C. Genes, D. Vitali, P. Tombesi, S. Gigan, and M. Aspelmeyer, Ground-state cooling of a micromechanical oscillator: Comparing cold damping and cavity-assisted cooling schemes, Phys. Rev. A **77**, 033804 (2008).
[43] F. Marquardt, J. P. Chen, A. A. Clerk, and S. M. Girvin, Quantum Theory of Cavity-Assisted Sideband Cooling of Mechanical Motion, Phys. Rev. Lett. **99**, 093902 (2007).
[44] I. Wilson-Rae, N. Nooshi, W. Zwerger, and T. J. Kippenberg, Theory of Ground State Cooling of a Mechanical Oscillator Using Dynamical Backaction, Phys. Rev. Lett. **99**, 093901 (2007).
[45] The linear entropy of a thermal state is given by $S_L = \mathrm{Tr}[1-\hat{\rho}^2] = \bar{n}_p/(\bar{n}_p + 1/2) \approx 2\bar{n}_p$ for low $\bar{n}_p$.
[46] S. Gröblacher, K. Hammerer, M. R. Vanner, and M. Aspelmeyer, Observation of strong coupling between a micromechanical resonator and an optical cavity field, Nature (London) **460**, 724 (2009).
[47] N. Rossi, B. Gross, F. Dirnberger, D. Bougeard, and M. Poggio, Magnetic force sensing using a self-assembled nanowire, Nano Lett. **19**, 930 (2019).
[48] F. R. Braakman and M. Poggio, Force sensing with nanowire cantilevers, Nanotechnology **30**, 332001 (2019).
[49] V. Jain, J. Gieseler, C. Moritz, C. Dellago, R. Quidant, and L. Novotny, Direct Measurement of Photon Recoil from a Levitated Nanoparticle, Phys. Rev. Lett. **116**, 243601 (2016).
[50] G. A. Brawley, M. R. Vanner, P. E. Larsen, S. Schmid, A. Boisen, and W. P. Bowen, Nonlinear optomechanical measurement of mechanical motion, Nat. Commun. **7**, 10988 (2016).
[51] P. Weber, J. Güttinger, A. Noury, J. Vergara-Cruz, and A. Bachtold, Force sensitivity of multilayer graphene optomechanical devices, Nat. Commun. **7**, 12496 (2016).
[52] E. E. Wollman, C. U. Lei, A. J. Weinstein, J. Suh, A. Kronwald, F. Marquardt, A. A. Clerk, and K. C. Schwab, Quantum squeezing of motion in a mechanical resonator, Science **349**, 952 (2015).
[53] F. Lecocq, J. B. Clark, R. W. Simmonds, J. Aumentado, and J. D. Teufel, Quantum Nondemolition Measurement of a Nonclassical State of a Massive Object, Phys. Rev. X **5**, 041037 (2015).